

# Investigation of 3-D RCS Image Formation of Ships Using ISAR

Richard T. Lord, University of Cape Town (UCT), South Africa

Willie Nel, Council for Scientific and Industrial Research (CSIR), South Africa

Mohammed Y. Abdul Gaffar, Council for Scientific and Industrial Research (CSIR), South Africa

## Abstract

Conventional Inverse Synthetic Aperture Radar (ISAR) utilises the rotational motion of a target such as a ship or an aircraft to obtain a 2-D image of the target's radar cross section (RCS) profile from a coherent radar system. This concept can be extended to obtain a 3-D RCS profile if the target's translational and rotational motion has the required attributes and is known with sufficient accuracy. This paper is a preliminary investigation to see whether 3-D ISAR images can be generated with a single antenna, using an approach that is different from interferometric ISAR. Simulation results have verified that 3-D ISAR images can be obtained under certain circumstances. A major problem experienced with ship ISAR data is multipath reflection off the sea surface. Simulations have been performed, which illustrate the degrading effect of specular multipath on the final 3-D image.

## 1 Introduction

ISAR is typically used to image targets such as aircrafts, ships and space objects that are important to both military and civilian communities. The rotational motion of the target creates a synthetic aperture that is utilised to obtain high cross-range resolution. The down-range resolution is achieved by transmitting a signal with a large bandwidth. Motion compensation is typically carried out to remove the effects of the targets translational motion from the target phase history [1]. ISAR applications include non-cooperative target recognition [2], measuring the RCS of a target [3], battlefield awareness [4], and the surveillance of ground traffic at airports, among others.

The motivation for this work originates from a hypothesis at the CSIR, that the phase histories of point-like target scatterers might be unique in all three dimensions, when a target, such as a ship at sea, exhibits significantly complex motion, including forward velocity, roll and pitch. In recent years there has been an interest in 3-D ISAR imaging [5–14]. The literature suggests that two different approaches have been taken to obtain 3-D ISAR images. These include interferometric ISAR [5–10], where multiple antennas are used, and 3-D ISAR where a single antenna is used [11–14]. According to [8], it is feasible to obtain 3-D ISAR images without knowledge of the target's motion, if three receivers are used. Interferometric methods possess undesirable qualities when compared to single-antenna 3-D ISAR techniques. One issue is the sensitivity to glint [15], and another issue is that interferometric ISAR only provides a single height

and RCS value for each  $x$ - $y$  cell in the 2-D image. Conversely, 3-D ISAR techniques using a single antenna provide a RCS value at different heights for each  $x$ - $y$  cell, thereby providing more information about the target.

For the 3-D ISAR approach, algorithms in [11] and [12] use many 2-D ISAR images to form a single 3-D image of the target. The algorithm in [13] is proposed for near-field turntable measurements, and it is assumed that the motion parameters are known. The technique that is proposed in [14] requires knowledge of the relative positions of the radar and target, the viewing angles of the measurements, and the corresponding 1-D range profile at these viewing angles. This paper addresses the issue of 3-D ISAR differently to existing work in the literature [11–14]. In the present work, a single antenna is used, positioned in the far field, and the 3-D ISAR image is formed without generating and merging intermediate 2-D images.

Section 2 describes the 3-D ISAR processing technique that was used and shows some of the simulation results that have been obtained. Section 3 investigates the effects of specular multipath on 3-D ISAR images of ship targets. In practice, only an estimate of the ship's motion profile would be used. This paper does not address the issue of using inaccurate motion parameters to form the 3D ISAR image. Other "real-life" effects not studied in detail here include target scintillation, target reflection directivity, multi-bounce effects and non-linear (frequency dispersive) scattering effects. These effects may lead to significant image degradation for complex target signatures.

## 2 3-D ISAR Processing

### 2.1 2-D ISAR processing revisited

ISAR utilises the relative motion between the radar antenna and the target to synthesise a longer aperture, which leads to an increase in the cross-range resolution. The maximum resultant cross-range resolution is directly proportional to the Doppler bandwidth  $B_d$ , which can be approximated by the difference between the maximum and minimum instantaneous Doppler frequency. Figure 1 illustrates a typical ISAR geometry for rotating targets. The radar antenna is pointing along the positive  $y$ -axis, at a distance  $R_0$  from the origin of the  $x$ - $y$  axes. A point target travels anti-clockwise along a semi-circle with radius  $r$  and an angular velocity  $\dot{\theta}$ . The antenna illuminates the target between  $t = t_1$  and  $t = t_2$ .

The phase history of such a target is given by

$$\phi(t, R_0, r) = \frac{-4\pi}{\lambda} \cdot \sqrt{r^2 + 2rR_0 \sin(\dot{\theta}t) + R_0^2}$$

The instantaneous Doppler frequency  $f_d(t, R_0, r)$  is obtained by taking the time derivative of the phase history. The equation for  $B_d$  can then be derived as

$$\begin{aligned} B_d &= f_d(t_2, R_0, r) - f_d(t_1, R_0, r) \\ &= \frac{-2rR_0\dot{\theta} \cos(\dot{\theta}t_2)}{\lambda \cdot R(t_2, R_0, r)} - \frac{-2rR_0\dot{\theta} \cos(\dot{\theta}t_1)}{\lambda \cdot R(t_1, R_0, r)} \end{aligned}$$

where  $R(t, R_0, r)$  is the expression for the range history. This expression for  $B_d$  can be simplified, if the target is being illuminated symmetrically about  $\theta = 90^\circ$ , such that the slant ranges at  $t_1$  and  $t_2$  are equal. In this case, assuming  $R_0 \gg r$  and that the argument of the sin term is small:

$$B_d \approx \frac{4r\dot{\theta} \sin\left(\frac{t_i \dot{\theta}}{2}\right)}{\lambda} \approx \frac{2r\dot{\theta}^2 t_i}{\lambda}$$

The cross-range resolution is then given by

$$\rho_a = \frac{r\dot{\theta}}{B_d} \cdot K_a \approx \frac{\lambda K_a}{2\dot{\theta} t_i}$$

Where  $K_a$  is a window broadening factor, which is 0.89 for a rectangular window. In order to focus the simulated ISAR data as accurately as possible, a time-domain ISAR processor was written, which takes as an input the 1-D range-compressed range profiles, and produces a fully-focussed 3-D image cube as an output. For each pixel in the 3-D cube, all the bins in the 1-D range-compressed range profiles belonging to this pixel's phase history are collected, phase-compensated and integrated. If a pixel in the 3-D

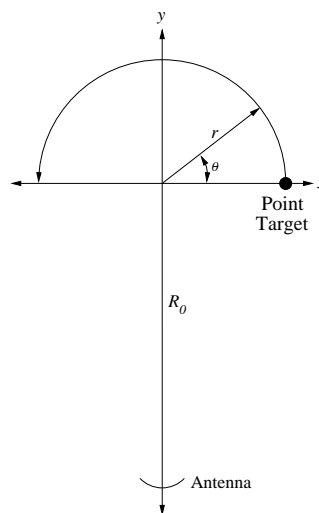


Figure 1: ISAR geometry for rotating targets.

cube corresponds to a true scatterer of the target, the integration of the phase-compensated bins produces a large value which is placed in that pixel.

### 2.2 3-D ISAR simulation setup

The above expression for the cross-range resolution is only valid if the target rotates around the  $z$ -axis (or, similarly, around the  $x$ -axis). Simulations were performed to investigate whether it is possible to achieve resolution enhancement in both the  $x$ - $y$  plane and the  $x$ - $z$  plane. In the simulation environment, the target rotates around two (or more) axes simultaneously. The sequence of rotation is first around the  $x$ -axis, then the  $y$ -axis and then the  $z$ -axis. The target was made up of a 3-D grid of  $5 \times 5 \times 3$  point targets. The target cluster was illuminated symmetrically about  $\theta = 90^\circ$ , with reference to Figure 1. The relevant parameters of this simulation are given in Table 1.

This cluster of point targets is shown in Figure 2 (a), which also depicts the effective axis of rotation, if the target cluster was rotating simultaneously around the  $y$ - and  $z$ -axes. The spacing between the point targets is 5m in all three dimensions, and the pixel size of the processed 3-D cube is 0.04m in all three dimensions.

Table 1: Radar and simulation parameters.

Parameter	Value
Centre frequency	10 GHz
Radar bandwidth	400 MHz
Complex sampling rate	500 MHz
PRF	100 Hz
Azimuth beamwidth	3 deg
Elevation beamwidth	3 deg
Distance from radar antenna to target	1000 m
Integration time	2 s
Rotational velocity around an axis	$10^\circ/\text{s}$

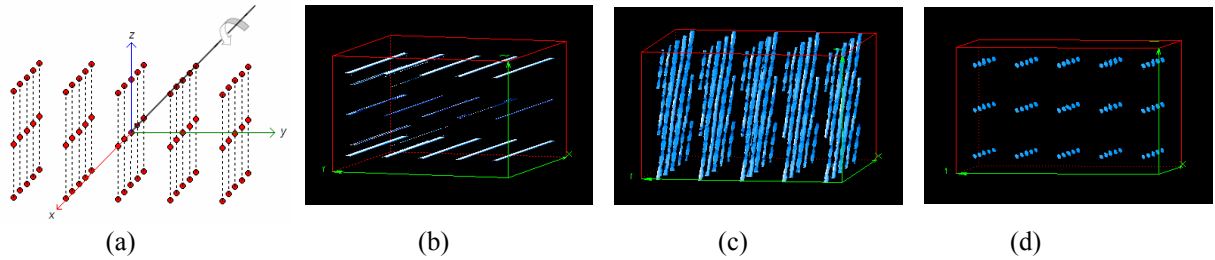


**Figure 2: 3-D views of processed image cubes of grid of point targets: (a) Original point target layout, (b) Rotation around  $x$ - and  $y$ -axes, (c) Rotation around  $x$ - and  $z$ -axes, (d) Rotation around  $y$ - and  $z$ -axes.**

### 2.3 Simulation results

Figure 2 shows 3-D views of the processed image cubes. In Figure 2 (b) the target cluster rotated simultaneously around the  $x$ - and  $y$ -axes, in (c) it rotated simultaneously around the  $x$ - and  $z$ -axes, and in (d) it rotated simultaneously around the  $y$ - and  $z$ -axes. From Figure 2 (d) it is clearly visible that the point targets have been resolved in all three dimensions! However, it is not obvious, how one would analytically predict the expected  $z$ -resolution. Analysis of the processed point targets showed that the resolution in the  $y$ -direction agreed very well with the predicted range resolution (in this case 0.33m) based on the radar bandwidth, and the resolution in the  $x$ -direction agreed very well with the predicted cross-range resolution (in this case 0.038m) based on the expression given in Section 2.1 and using the rate of rotation around the  $z$ -axis only. However, the measured resolution in the  $z$ -direction was only 0.42m. When the integration time was reduced to 1s, the measured resolution in the  $z$ -direction decreased to 1.69m, clearly much worse than the resolution obtained in the  $x$ -direction.

An attempt was made to predict the  $z$ -resolution by analysing the instantaneous Doppler frequency history. However, a problem arises when attempting to “split” the Doppler frequency history into components caused by movement in the horizontal plane (i.e. setting  $z = 0$ ), and movement in the vertical plane (i.e. setting  $y = 0$ ). This problem originates from the radar only being able to see two dimensions, namely range and cross-range. Work is currently continuing in finding analytical expressions for the expected  $z$ -resolution.

## 3 Multipath

Multipath is a major problem for radar applications in general. When imaging targets on the ocean surface with low grazing angles, the effects of diffuse and specular multipath can severely degrade the quality of the processed image. Here an attempt was made to simulate the effects of specular multipath, by carefully placing “ghost” targets in the simulation setup, which correspond to targets that the radar would see

due to reflections off the sea surface. Careful consideration was given to incorporating the antenna gain pattern and the magnitude of the Fresnel reflection coefficient  $\rho_0$  in order to scale the RCS of each point target correctly. Furthermore, the received signal at the radar antenna was phase-shifted appropriately according to the phase  $\phi$  of the Fresnel reflection coefficient. Table 2 summarises the values for the reflection coefficients that were used, based on values given in [16]. The grazing angle  $\psi$  is calculated from the ground-range distance  $R_0$  between radar and target, and the height of the radar  $h_r$ . Note that the magnitude of the reflection coefficient decreases significantly for vertical polarisation and larger grazing angles, and that the phase of the reflection coefficient at these grazing angles is close to zero degrees, and not  $180^\circ$ .

Figure 3 shows the front and side views of the ship model that was assembled, which consisted entirely of point targets. Some point targets have short lines protruding from them, indicating that their RCS reflectivity is directional, based on a cosine distribution. All targets have a RCS with a standard deviation of 5%, in order to simulate amplitude fluctuation of scatterers. All simulations were performed by rotating the ship model around the  $y$ - and  $z$ -axes, and, where relevant, the same parameters listed in Table 1 were used.

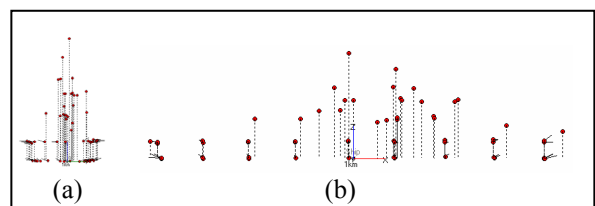


**Figure 3: (a) Front and (b) side view of ship model.**

**Table 2: Fresnel reflection coefficients used.**

$Pol.$	$R_0$ [km]	$h_r$ [m]	$\psi$	$\rho_0$	$\phi$
HH	3	10	$0^\circ$	0.97	$180^\circ$
HH	3	1000	$18.4^\circ$	0.90	$180^\circ$
HH	6	10	$0^\circ$	0.97	$180^\circ$
HH	6	1000	$9.5^\circ$	0.96	$180^\circ$
VV	3	1000	$18.4^\circ$	0.40	$0^\circ$
VV	6	1000	$9.5^\circ$	0.20	$0^\circ$

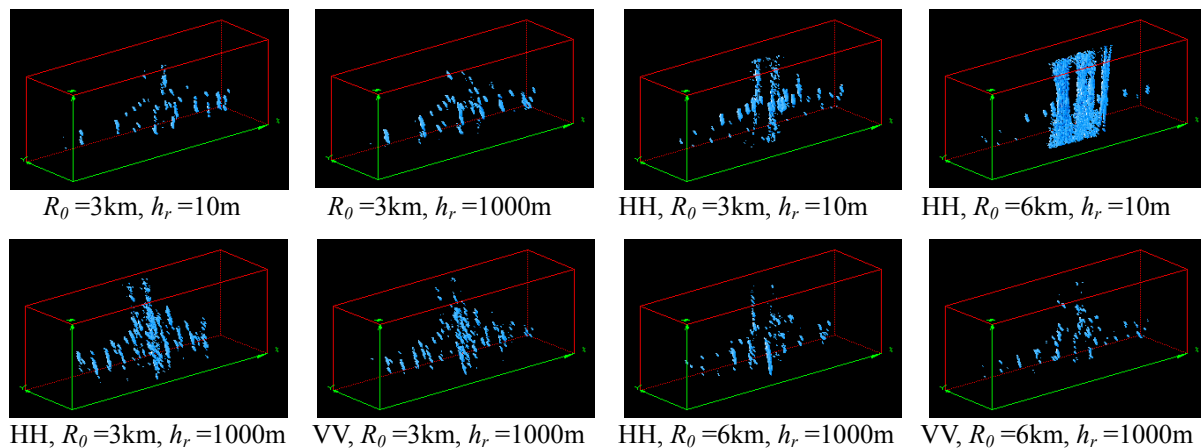


Figure 4: Simulation results showing effect of multipath on 3-D image of ship target.

Figure 4 shows 3-D views of the processed ship simulation. The first two images in the top row do not include multipath effects, in order to serve as a benchmark. All simulations that include multipath show a definite decrease in image fidelity. It is interesting to note that the VV polarised images at a radar height of 1000m (bottom row) seem slightly better than their HH counterparts, which would agree with their lower reflection coefficient value.

## 4 Conclusions

Simulations have verified that it is possible to obtain 3-D RCS images of targets using ISAR, if the target motion profile meets certain requirements. These requirements are met when the target is rotating around the local  $y$ - and  $z$ -axes simultaneously, as defined in this paper. However, other, more complicated manoeuvres, including combinations of linear and rotational motion, can also produce 3-D resolution. Unfortunately, the obtained height resolution does not seem to be as good as the cross-range resolution one normally obtains with 2-D ISAR. It is convenient to process ISAR data using the flexibility of a time-domain processor. Further work is currently underway to find analytical expressions for the expected height resolution, given certain target motion profiles. Simulations have also verified that multipath severely affects the final image quality of ship targets, and that VV is the preferred polarisation for imaging ships on the ocean.

## References

- [1] Li, J.; Wu, R.; Chen, V.C.: *Robust autofocus algorithm for ISAR imaging of moving targets*. IEEE Transactions on Aerospace and Electronic Systems, 37 (3), 2001, pp. 1056–1069.
- [2] Menon, M.M.; Boudreau, E.R.; Kolodzy, P.J.: *An automatic ship classification system for ISAR imagery*. The MIT Lincoln Laboratory Journal, 6 (2), 1993, pp. 289–308.
- [3] Jain, A.; Patel, I.: *Dynamic imaging and RCS measurements of aircrafts*. IEEE Transactions on Aerospace and Electronic Systems, Vol. 20, 1984, pp. 363–399.
- [4] Fennel, M.T.; Wishner, R.P.: *Battlefield awareness via synergistic SAR and MTI exploitation*. IEEE Transactions on Aerospace and Electronic Systems, 13 (2), 1998, pp. 39–45.
- [5] Xiaojian, X.; Narayanan, R.M.: *Three-dimensional interferometric ISAR imaging for target scattering diagnosis and modelling*. IEEE Transactions on Image Processing, 10 (7), 2001, pp. 1094–1102.
- [6] Xiaojian, X.; Hong, L.; Peikang, H.: *3-D interferometric ISAR images for scattering diagnosis of complex radar targets*. IEEE Radar conference, April 1999, pp. 237–241.
- [7] Xu, X.; Narayanan, R.M.: *Enhanced resolution in 3-D Interferometric ISAR Imaging using an iterative SVA procedure*. Int. Geoscience and Remote Sensing Symposium, Vol. 2, July 2003, pp. 935–937.
- [8] Wang, G.; Xia, X.G.; Chen, V.C.: *Three-dimensional ISAR imaging of maneuvering targets using three receivers*. IEEE Trans. on Image Proc., 10 (3), March 2001, pp. 436–447.
- [9] Xu, X.; Narayanan, R.M.: *Three-dimensional interferometric ISAR imaging for target scattering diagnosis and modelling*. IEEE Trans. on Image Proc., 10(7), July 2001, pp.1094–1102.
- [10] Zhang, Q.; Yeo, T.S.; Du, G.; Zhang, S.: *Estimation of three-dimensional motion parameters in interferometric ISAR imaging*. IEEE Transactions on Geoscience and Remote Sensing, 42 (2), Feb 2004, pp. 292–300.
- [11] McFadden, F.E.: *Three dimensional reconstruction from ISAR sequences*, Proc. of SPIE, Vol. 4744, 2002, pp. 58–67.
- [12] Mayhan, J.T.; Burrows, M.L.; Cuomo, K.M.: *“High resolution 3D snapshot” ISAR imaging and feature extraction*. IEEE Transactions on Aerospace and Electronics Systems, 37 (2), 2001, pp. 630–642.
- [13] Fortuny, F.: *An efficient 3-D near field ISAR algorithm*. IEEE Transaction on Aerospace and Electronics Systems, Vol. 34, 1998, pp. 1261–1270.
- [14] Knoell, K.K.; Cardillo, G.P.: *Radar tomography for the generation of three-dimensional images*. Proc. Inst. Elec. Eng. Radar Sonar Navigation, 142 (2), 1995, pp. 54–60.
- [15] Weng-Rong, W.: *Target tracking with glint noise*. IEEE Trans. on Aerospace and Electronic Systems, 29 (1), 1993, pp. 174–185.
- [16] Barton, D.K.: *Modern Radar System Analysis*. Artech House, 1988.